RJC

RASĀYAN ***J. Chem.***
Vol. 11 | No. 1 |53-62 | January - March | 2018
ISSN: 0974-1496 | e-ISSN: 0976-0083 | CODEN: RJCABP
http://www.rasayanjournal.com
http://www.rasayanjournal.co.in

HYDROTHERMAL SYNTHESIS OF ULTRA VIOLET-VISIBLE LIGHT RESPONSIVE RUTHENIUM DOPED TITANIA ($Ru_XTi_{1-X}O_2$) NANOSHEET AND ITS EFFECT ON PHOTOCATALYTIC DEGRADATION OF REACTIVE RED DYES

Ashwini Ashok[1], Kalaivani Raman[1,*], Shanmugaraj Andikkadu Masilamani[2] and Raghu Subash Chandra Bose[2]

[1]Department of Chemistry, Vels University, Pallavaram, Chennai-600117, Tamil Nadu,India.
[2]Centre for Advanced Research & Development (CARD), Vels University, India.
*E-mail: rakvani@yahoo.co.in

ABSTRACT

In the present work, ruthenium doped titania ($Ru_XTi_{1-X}O_2$) nanosheet was synthesized by hydrothermal method using titanium tetraisopropoxide and ruthenium trichloride trihydrate as metal precursors. The structural, chemical and morphological properties were determined using X-Ray diffraction (XRD), X-ray photoelectron spectroscopy (XPS) and Transmission electron microscopy (TEM). The synthesized$Ru_XTi_{1-X}O_2$ nanocrystals were used as photocatalyst for the degradation of Reactive Red 198 (RR) dye in aqueous solutions at the room temperature. The photocatalytic activity of the $Ru_XTi_{1-X}O_2$ nanosheet was evaluated and compared with its control counterpart TiO_2. Significant improvement in dye degradation is noted for $Ru_XTi_{1-X}O_2$, when compared to TiO_2. Which is corroborated to the increased visible light absorption due to the presence of ruthenium in the crystallite sites of TiO_2 that resulted in well separated photo-generated electron and hole pairs under the light illumination.

Keywords: hydrothermal process, titania nanocrystal, ruthenium dioxide, wastewater treatment, photocatalysis.

INTRODUCTION

Every year approximately 300,000 tons of synthetic organic contaminants (SOC) have been released into the water around the world.[1] Synthetic organic contaminants (SOC), which include organic dyes, are the major sources of environmental pollution that ultimately leads to health risks in water supply systems. Among the various methods of SOC treatment, an advanced oxidation process (AOP) has observed to be effective in organic dye degradation and detoxification of contaminated water.[2] Even among the various types of AOPs, Photocatalytically induced oxidation is considered to be an efficient method as the organic pollutants are completely converted into harmless species without the need of chemical oxidizing agents such as hydrogen peroxide (H_2O_2).[2,3] Nanostructured semiconductor photocatalysts such as Titania (TiO_2) based have been widely employed in organic dye degradation due to its physical and chemical stability, excellent photocatalytic activity, low cost and ease of production.[4] Though, TiO_2 is observed to be efficient photocatalyst for dye degradation, its activity is limited to ultraviolet (UV) regime with fairly poor degradation in visible regime due to its wide band gap (3.0~3.5 eV) and short diffusion length of photoinduced electron-hole pairs[5]. By introducing heteroatoms as a dopant, the electron concentration, mobility and lifetime of the charge carriers in TiO_2 can be effectively tuned.[5,6] Also, the introduction of dopants alters the electronic structure with the re-alignment in the band levels due to the formation of donor or acceptor levels in between the valence band maximum (VBM) and conduction band minimum (CBM), consequently induces visible light absorption and thereby improved photocatalytic activity in the visible regime.[5] Extensive research has been done to improve the photocatalytic performance of TiO_2 in

the visible regime by doping heteroatoms including metal (Fe, Cr, Co, Cu, Ru and Ag) and non-metals (S, C, N), which helps in re-aligning the band edge with well separated electron-hole pairs.[7-12]

For example, Chao *et al.*(2003) studied the effect of silver (Ag) doping onTiO_2 and reported a significant rise in the specific surface area of TiO_2 particles, which ultimately resulted in improved photocatalytic activity in the visible regime.

Among the various dopants, ruthenium (Ru) is considered as efficient metal dopant as it leads to well separated electron-hole pair with widened photoabsorption characteristics in the visible regime even at lower dopant concentration. Significant research has been done on the synthesis and photocatalytic performance of ruthenium doped TiO_2.[13-18] For example, a report by senthilnathan *et al.*, corroborated significant rise in visible light responsive photocatalytic performance is noted on doping Ru with the rise in dye removal efficiency from 40 (TiO_2) to 80 % (Ru-TiO_2).[18] However, interestingly no systematic investigation has been made on the shape-controlled synthesis of ruthenium doped TiO_2 and its photocatalytic performance. An earlier report by Shengchao Nie *et al.*[19], revealed that photocatalytic performance of TiO_2 can be altered by tuning the shape of the TiO_2.

In this report, an attempt has been made to synthesize ruthenium doped titania ($Ru_XTi_{1-X}O_2$) hydrothermally using titanium and ruthenium salt as precursors in the presence of capping surfactants such as oleic acid (OA) and oleylamine (OM). The synthesized photocatalyst was characterized using X-ray diffraction (XRD), X-ray photoelectron spectroscopy, transmission electron microscopy (TEM) and UV-visible spectroscopy. Finally, the photocatalytic degradation behavior of the visible light responsive $Ru_XTi_{1-X}O_2$ was investigated using reactive red dye effluent.

EXPERIMENTAL

Materials

Titanium (IV) isopropoxide (TIP, 97%), ruthenium (III) chloride hydrate and reactive red were obtained from Sigma-Aldrich, India. Ethanol, Oleylamine (OM), oleyl acid (OA) and hydrogen peroxide (H_2O_2) were procured from Merck India Ltd. All used chemicals were of analytical grade. The glassware used in all the experiments were made up of Schott Duran.

Preparation of Ru-doped TiO_2

UV and visible light responsive nanostructured ruthenium doped titania ($Ru_XTi_{1-X}O_2$) with the mole ratio of 3:97 (Ru:Ti) was synthesized via.hydrothermal method by slightly modifying the procedure reported by Nie *et al.*[19] In the typical synthesis, a known quantity of titanium isopropoxide (0.97 moles) and ruthenium chloride (0.03 moles) were added to 30 mL of ice-cold distilled water (ca.0–5^oC) under the continuous stirring condition for 3 hrs followed by sonication for 30 minutes using bath sonicator (Bath sonicator 1.5L 50H) . After sonication, 10 mL of OA and 5 mL of OM were added to the solution and subsequently kept the solution under the stirring condition for 12 hrs. To the resultant heterogeneous mixture, the calculated amount of ammonia was slowly added, until pH of ca.7 was reached. The brown colored suspension was kept in ideal condition for 12 hrs, which was then filtered and cleaned for several times using de-ionized water. The obtained brown precipitate was dispersed in cold distilled water (4^o C) and subsequently mixed with 50 mL of 30 % H_2O_2 solution. The resulting solution was kept under stirring condition (30 min) followed by sonication using bath sonicator (30 min). Then, 20 mL of the ruthenium/titania sol was heated in a teflon coated steel autoclave maintained at 180^{o}C for 5 hrs. The resulting yellowish brown colored samples were washed with ethanol several times to remove any physically adsorbed organic surfactants followed by drying under vacuum. The obtained yellowish dark brown powder was subjected to calcination at 600^o C for 6 hrs in argon atmosphere using the tubular furnace to remove the impurities. Finally, to yield dark brown colored ruthenium doped titania ($Ru_xTi_{1-x}O_2$) samples.

Characterization

X-ray diffraction (XRD) patterns of the synthesized ($Ru_XTi_{1-X}O_2$) photocatalyst were obtained in the 2θ range of 20~80º using X'Pert Pro (PANalytical) diffractometer (CuKα, 20 kV) set at the scanning step

interval of 0.04°/sec. The morphological features of the synthesized catalyst were determined using transmission electron microscope (JEOL 2100, Japan) equipped with field emission electron source operated at 200 kV. UV-Vis diffuse reflectance measurements of synthesized photocatalyst were performed in the spectral range of 200 to 900 nm on DH-2000 BAL spectrasuite (Ocean Optics, USA) spectrophotometer. Survey and high-resolution XPS spectra of synthesized photocatalyst were collected using SHIMADZU ESCA 3400 (Japan). The photocatalytic dye degradation experiments were performed using Phillips UV lamp (8" 11W Philips UV Lamp, India) and 11W visible light lamp (FL10D,Wooree Lighting Co). The concentration gradient of the dye solutions was recorded in UV-Vis spectrophotometer (DH-2000 BAL spectrasuite spectrometer, ocean optics, USA). Distilled water was used as a reference in UV measurements.

Photocatalytic Activity

The photocatalytic dye degradation behavior of the synthesized ($Ru_XTi_{1-X}O_2$) samples was determined by exposing the mixture of catalyst and an aqueous solution of reactive red under UV and visible light. Typically, 80 mg of photocatalyst powder was added to the 80 mL of dye solution (20 mg/L). Before irradiation, the suspensions were sonicated for 3 min and then magnetically stirred in dark environment for 30 min to establish adsorption / desorption equilibrium. The suspension was then irradiated under a UV / visible lamp for different time intervals. About 3 mL of the irradiated sample was taken at regular time intervals from the catalyst-dye suspension and centrifuged at 2000 rpm for 4 minutes to remove the photocatalyst powders. The UV-Vis absorption spectra of the centrifuged solutions were recorded to determine the dye concentration.

RESULTS AND DISCUSSION

The pictorial representation of peroxide sols, a heterogeneous solution containing nanocrystals after the hydrothermal treatment and the toluene dispersion of the nanocrystals are shown in Fig.-1. While the Fig.-1(a-c) shows the pictures of titanium peroxide sol (a), heterogeneous solution (b) and toluene dispersion of titania (TiO_2) crystals (c), Fig.-1(d-f) represents the peroxide sols of titanium and ruthenium (d), a heterogeneous solution containing $Ru_XTi_{1-X}O_2$ (e) and its toluene dispersion (f). Shown in Fig.-1(a, d) is the isopropanol (IPA) based peroxide sols of titanium (transparent yellow) and titanium/ruthenium mixture (brown), which are very stable and can be kept for several weeks at room temperature in an air atmosphere. Upon hydrothermal treatment, the yellow/brown colored transparent solution changed to a mixture consisting of two layers as shown in Fig.-1(b and e). The top and bottom layers correspond to organic layers (OA & OM) in IPA (top layer) and the light grey colored TiO_2 (Fig.-1b) / $Ru_XTi_{1-X}O_2$ (Fig.-1e) nanocrystal dispersion (bottom layer), respectively. Since, both the synthesized TiO_2/$Ru_XTi_{1-X}O_2$ are capped with hydrophobic OA and OM molecules, they exist between the oil and water layers making it as a two-layer mixture as shown in the Fig.-1(b and e). After hydrothermal treatment, the bottom layer consisting of TiO_2/$Ru_XTi_{1-X}O_2$ was carefully collected after removing the top and bottom layer, which was subsequently washed several times with ethanol to remove physically absorbed OA and OM molecules. The samples were then calcined at 600°C for 6 hrs in an argon atmosphere. The obtained powders of TiO_2 (grey colored) and $Ru_XTi_{1-X}O_2$(brown colored) were dispersed in toluene (0.1 mg/mL) to get stable dispersion as shown in Fig.-1(c and f).

Figure-2a shows the rutile crystal structures of bulk titania (TiO_2) and ruthenium oxide (RuO_2). The tetragonal bulk unit cell structure is similar in both the TiO_2 and RuO_2 nanostructures, when both the metals exist in +4 oxidation states (Ti^{4+}; Ru^{4+}) with the coordination number of 6. Though the segregations of RuO_2 and TiO_2 phases during anatase to rutile phase transformation is possible, it is less feasible in the present work, since the concentration of Ru^{4+} is limited to 3 %. An earlier report by Nguyen-Phan *et al.*[20] revealed that the segregation of individual oxide is not possible if the concentration is less than 5 % as the solid solubility occurs below this level. Also, the difference in effective ionic radius of Ru^{4+} (62 pm) and Ti^{4+} (60.5 pm) is relatively smaller (only ~2.4 %) in the six coordination site of the rutile structure. The theoretical model of crystal structure and its XRD patterns proposed by corroborates no significant variation in crystal structure as well as its pattern is noted on doping low concentration of Ru in TiO_2 crystal planes. In the present investigation[20] the above discussion is valid

since the mole percentage of ruthenium is ≤3%. Figure-2b shows the XRD patterns of titania (TiO_2) and Ru doped titania ($Ru_XTi_{1-X}O_2$) crystals.XRD results revealed the presence of both anatase and rutile type in the synthesized titania samples (Fig.-2b). The appearance of diffraction peaks at 13.1° (110) and at 16.9° (101), whereas single broad transition at 13.5° (110) is observed in TiO_2 sample corroborating the existence of tetragonal rutile type crystals (Fig.-2b). An earlier report by Houskova[17] stated that ruthenium can assist anatase-to-rutile phase transformation at much lower temperatures in $Ru_XTi_{1-X}O_2$, when compared to titania (TiO_2) and this fact is correlated to the strong-metal-transport interaction. Absence of RuO_2 diffraction patterns in $Ru_XTi_{1-X}O_2$ is ascribed to the fine dispersion of ultra-small, sub-atomic RuO_2 clusters in TiO_2 clusters as well as its inclusion in host TiO_2 matrix.[21]

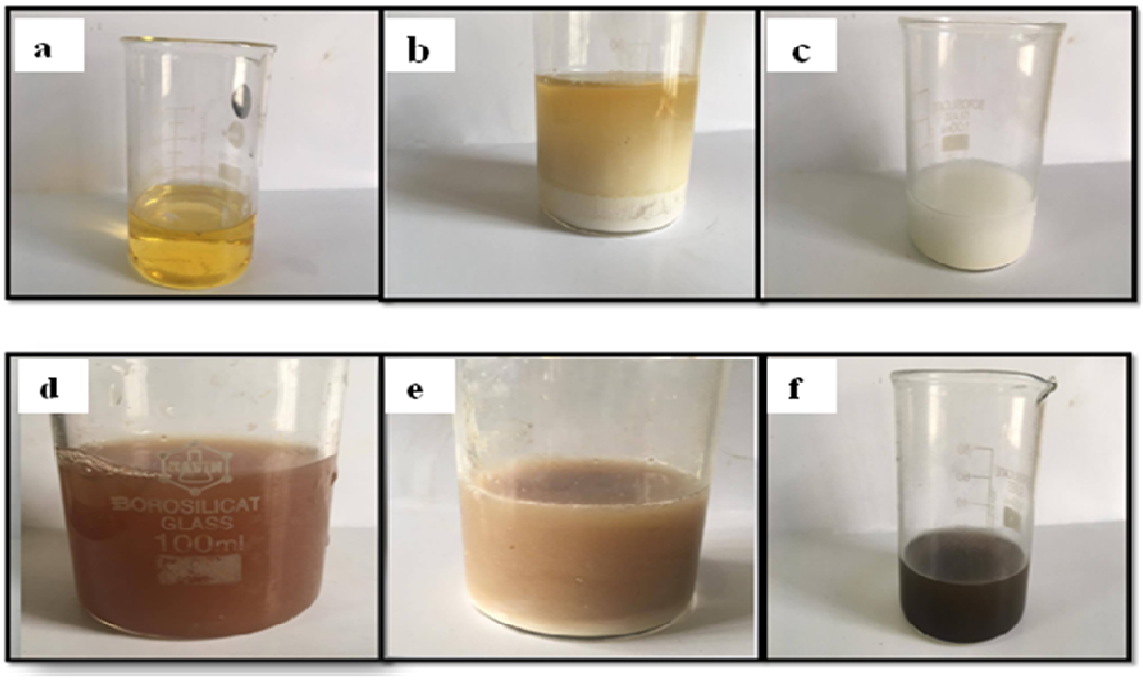

Fig.-1: The image of peroxide sols, heterogeneous solution containing nanocrystals after the hydrothermal treatment and the toluene dispersion of the nanocrystals (a) yellow transparent Titanium sol (b) heterogeneous mixture of titania (TiO_2) crystals (c) stable dispersion of (TiO_2) crystals, (d) brown coloured titania ruthenium sol_2 (e) heterogeneous mixture of ruthenium doped titania($Ru_XTi_{1-X}O_2$) crystals (f) stable dispersion of $Ru_XTi_{1-X}O_2$

Substitution of ruthenium ions (Ru^{4+}) into the TiO_2 lattice might also result in larger lattice constants and d-spacing values due to the relatively higher ionic radius of Ru^{4+} (62 pm) than that of Ti^{4+} in the hexa-coordination of the rutile structure. In the present work, the average d-spacing value calculated using (110) crystal plane of TiO_2 and $Ru_XTi_{1-X}O_2$ are observed to be 6.6 Å and 6.8 Å, which clearly supports the above fact. Alternatively, the strong diffraction patterns in the 2θ range of 25~80° revealed the existence of anatase type in the synthesized TiO_2 crystals. An earlier report by Shengchao[19] corroborated that relative concentration of oleic acid (OA) and oleylamine (OM) plays the vital role in the shape-controlled synthesis of titania crystals. According to their report, diffractive intensity ratio (101) and (004) peaks are significantly higher for nanosheet structured TiO_2 crystals. In the present investigation, OA and OM concentrations were fixed at 10 and 5 mL, which in turn should result in nanosheet structures of TiO_2 and this fact is well supported by the significantly higher value of diffractive intensity ratio of (101)/(004) crystal planes (~3.6) for titania samples (Fig.-1b). Though, $Ru_XTi_{1-X}O_2$ samples also exhibit similar diffraction pattern in the 2θ range of 25~79°, the peak corresponding to (004) plane becomes broadened with the complete disappearance of (002) and (011) crystal planes (Fig. 2b). Also, the diffraction peaks corresponding to (211) and (202) planes overlapped with (220) and (222) crystal planes. This fact is again

attributed to the introduction of ruthenium (Ru^{4+}, ionic radius 62 pm) ions replacing the titanium ions (Ti^{4+}, 60.5 pm), which in turn hampers the crystal grain growth in certain planes due to the formation of Ti-O-Ru bonds.[22] No significant variation in the diffractive intensity ratio of (101)/(004) crystal planes (~3.2) is noted for $Ru_XTi_{1-X}O_2$, when compared to TiO_2 corroborating the formation of nanosheet structures. This fact is further confirmed by the TEM images that displayed nanorod (rutile type crystals[20] and nanosheet (anatase type crystals[19] morphologies for both TiO_2 and $Ru_XTi_{1-X}O_2$ samples[23] (Fig.-3a and b).

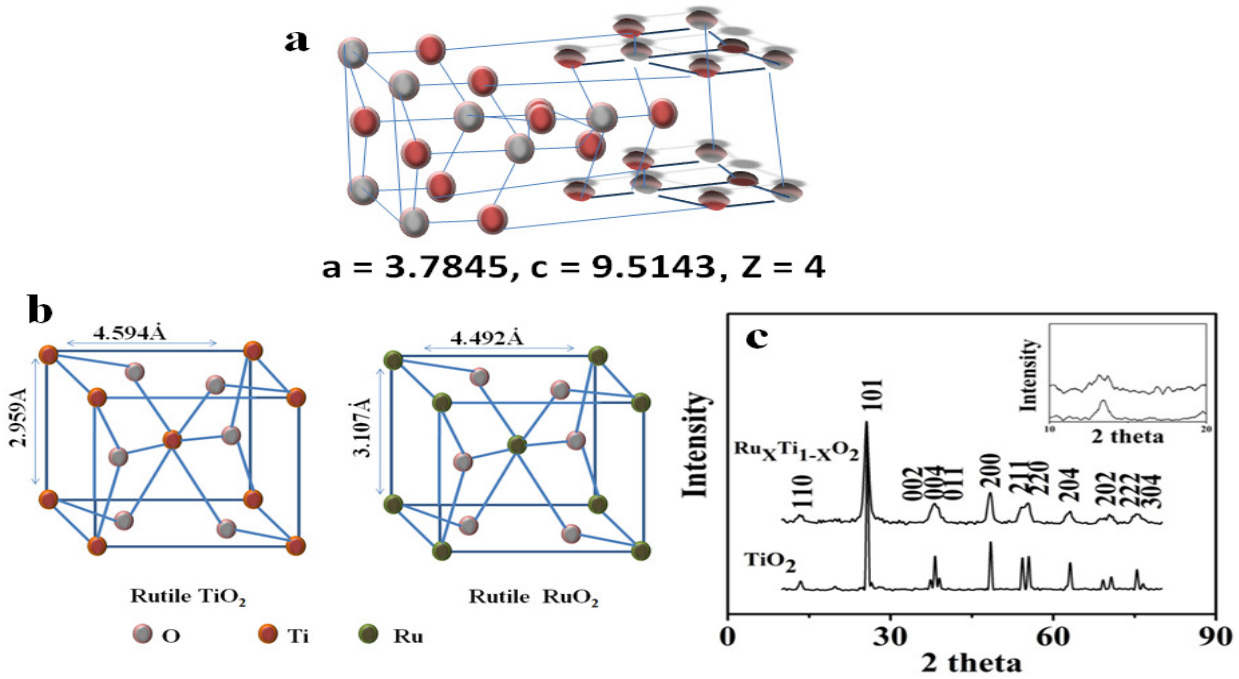

Fig.-2: (a) crystal structure of rutile TiO_2 (b) crystal structure of rutile TiO_2 and rutile RuO_2 (c) XRD patterns of titania (TiO_2) and Ru doped titania ($Ru_XTi_{1-X}O_2$) crystals.

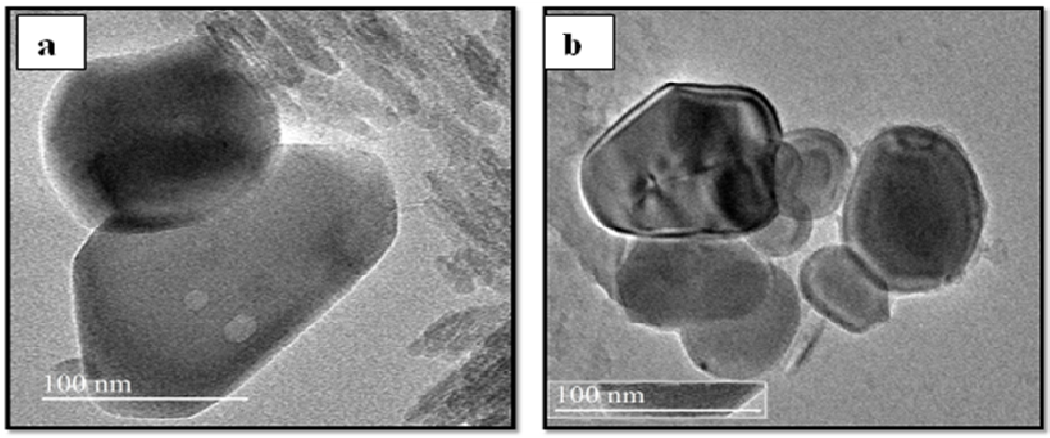

Fig.-3: TEM micrograph of titania (TiO_2) and Ru doped titania ($Ru_XTi_{1-X}O_2$) crystals.

Interestingly, surface distortions are noticed in $Ru_XTi_{1-X}O_2$ samples (Fig.-3b), when compared to titania samples (TiO_2) and this fact may be attributed to the introduction of low (Ru^{5+}, ionic radius, 58 pm) and high (Ru^{3+}, ionic radius, 68 pm) ionic radii ruthenium ions in the interstitial positions of crystal planes that resulted in buckled nanosheet morphology as proposed in the schematic representation (Fig.-4).

To understand the electronic structure and chemical states in the $Ru_XTi_{1-X}O_2$ nanosheets, XPS characterization was performed and the results are displayed in Fig.-5. The survey scan result of $Ru_XTi_{1-X}O_2$ confirms the presence of titanium, ruthenium and oxygen atoms as well as complete removal of chlorine atoms during the hydrothermal synthesis (Fig.-5a). High-resolution Ti2p spectra showed two peaks at 458.2 and 464.1 eV that corresponds to $Ti2p_{3/2}$ and $Ti2p_{5/2}$ corroborating the formation of an octahedrally coordinated Ti^{4+} state (with spin-orbit splitting Δ of 5.9). This result is quite consistent with the results reported by Nguyen-Phan *et al.*[20] and it may be attributed to the non-stoichiometric bonding of titanium to oxygen atoms through the substitution of Ru ions into the TiO_2 lattice.[24] High-resolution Ru_3d spectra showed a strong peak at around 285 eV (Ru $3d_{3/2}$) with a small broad hump at around 280 eV (Ru $3d_{5/2}$), implying the presence of Ru^{n+} (n = 2~5) in the interstitial positions along with the presence of Ru^{4+} state in the crystal lattice.

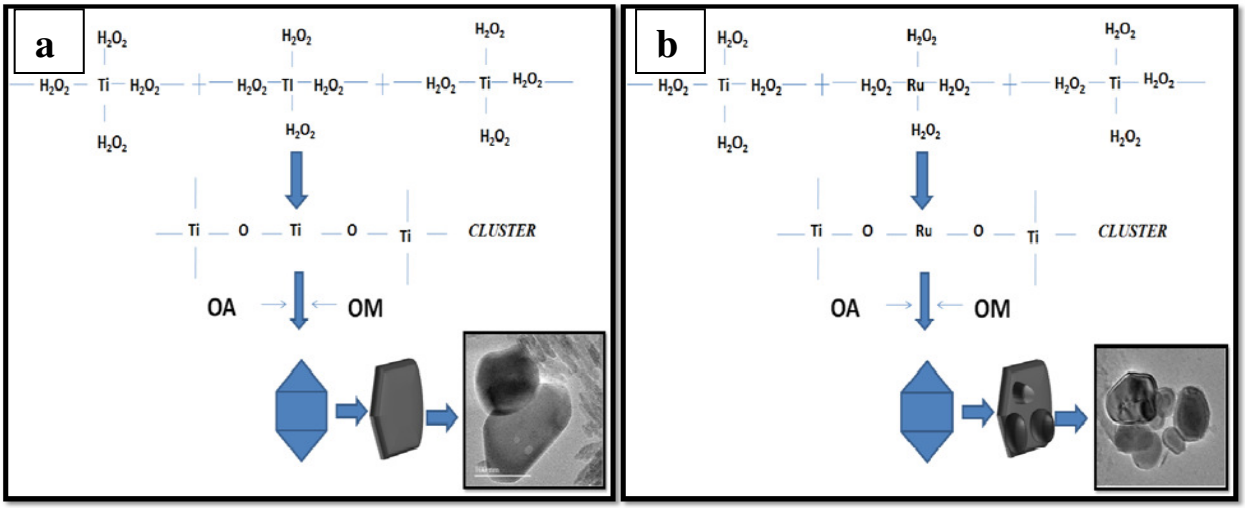

Fig.-4: Diagrams of the titania (TiO_2) and Ru doped titania ($Ru_XTi_{1-X}O_2$) crystals growth

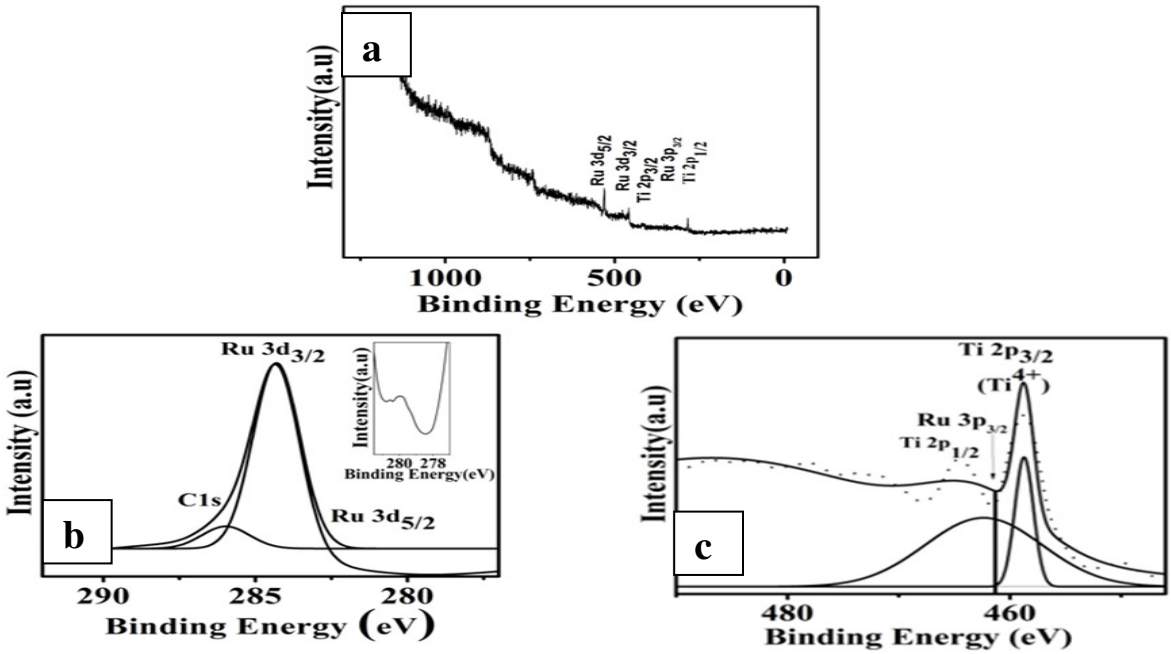

Fig.-5: High-resolution XPS core-level spectra of Ru doped titania ($Ru_XTi_{1-X}O_2$) crystal.

The overall photocatalytic performance of $Ru_XTi_{1-X}O_2$ depends on the oxidation states of ruthenium. While the replacement of Ti^{4+} with Ru^{4+} in the crystal lattice might induce an acceptor level in the band gap of TiO_2, presence of Ru^{3+} and Ru^{5+} in the interstitial positions induces both electron donor and acceptor levels in the band gap of TiO_2 to maintain the charge balance, which in turn resulted in a visible light response as well as significant impact in charge transport and its transfer pathway.[25]

The photocatalytic degradation of dye using synthesized catalyst depends on its light absorption behavior and the subsequent photoexcitation generating charge carriers. For understanding the visible light activated performance of a synthesized catalyst, optical property measurements were done using UV-Vis diffused absorption spectroscopy and the result is shown in Fig.-6. As reported by several researchers[20,26-28] , we also noticed an intense absorption in the range of 200~420 nm and it is attributed O_2p-Ti 3d transition (from the valence band to conduction band) and the onset located at around 450 nm that corresponds to the band gap energy of 2.76 eV for the synthesized $Ru_XTi_{1-X}O_2$ samples. Also, the visible absorbance in the range of 450~900 nm is significantly higher for the synthesized material and it can be corroborated to the charge transition of the donor ($Ru^{4+} \rightarrow Ru^{5+}+e^-$; $Ru^{3+} \rightarrow Ru^{4+}+e^-$) or acceptor ($Ru^{3+} \rightarrow Ru^{4+}+h^*$).[20]

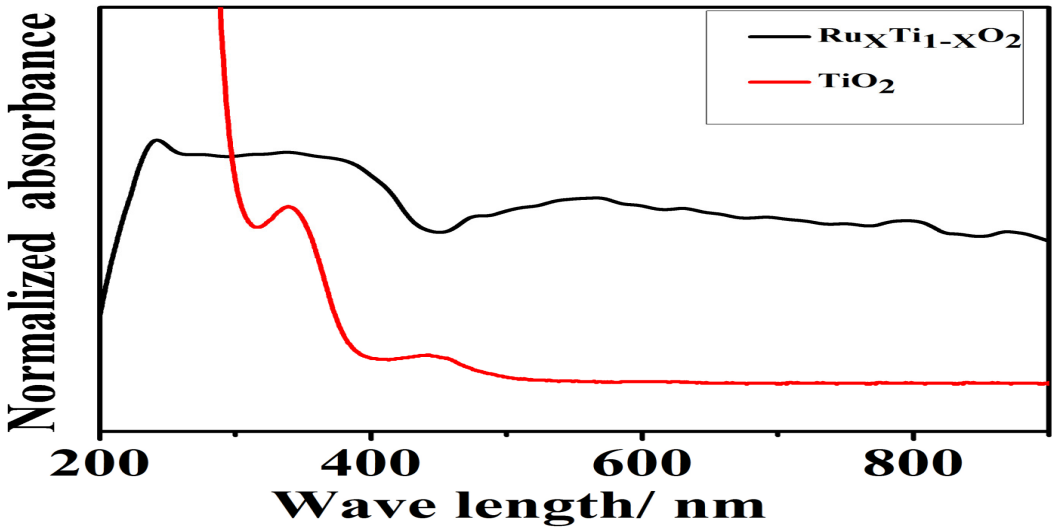

Fig.-6: UV-Vis diffused absorption spectra of Ru doped titania ($Ru_XTi_{1-X}O_2$) crystal.

Finally, the UV and visible light driven photocatalytic response of the synthesized $Ru_XTi_{1-X}O_2$ catalyst was carried out using the mixture of reactive red (RR) dye solution (20 ppm) and the synthesized catalyst (1g/Lt). For comparison purpose, photocatalytic degradation performance of titania (TiO_2) was also done using the same concentrations of RR dye (20 ppm) solution and the catalyst (1g/lt). From the results, one can notice that the synthesized material exhibit significantly higher degree of dye degradation both in UV and visible region, when compared to the pure titania catalyst (Fig.-7). For instance, dye degradation is observed to be 99 % on exposing the RR dye/$Ru_XTi_{1-X}O_2$ catalyst mixture to UV light for 150 min, whereas maximum degradation is noted to be only 71.2 % for RR dye/TiO_2 catalyst mixture. Similarly, a significant rise in dye degradation is noted for RR dye/$Ru_XTi_{1-X}O_2$ catalyst mixture (99 %) on exposing under visible light for 150 min in comparison to RR dye/TiO_2 catalyst mixture (10 %). From the results, it is quite evident that dye degradation performance is relatively better both in UV and visible light on doping ruthenium in titania catalyst ($Ru_XTi_{1-X}O_2$). Previous studies showed that anatase phase of titania has a higher photocatalytic activity than rutile phase and it can be attributed to the presence of a higher degree of surface hydroxyl groups.[29,30] Though the shape-controlled synthesis of TiO_2 and $Ru_XTi_{1-X}O_2$ resulted in anatase and rutile type phases, the significantly higher concentration of anatase type revealed that surface hydroxyl group catalyzed photocatalytic degradation mechanism proposed by Nagaveni *et al.*[30] is quite valid in the present systems. However, higher degradation rate exhibited by $Ru_XTi_{1-X}O_2$

especially under visible light may be correlated to the variation in the electronic structure due to the Ru doping.

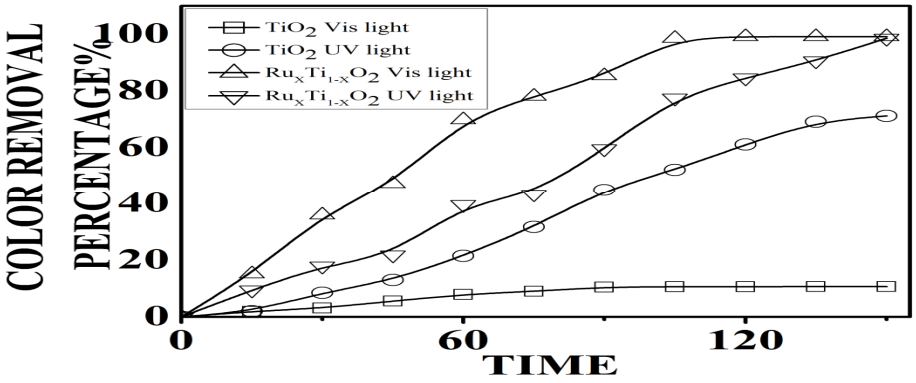

Fig.-7: Photocatalytic performance the $Ru_XTi_{1-X}O_2$ catalyst comparing with TiO_2 under UV/ Visible light region

Figure-8 shows the schematic representation of the proposed charge-transfer mechanism in $Ru_XTi_{1-X}O_2$. The interstitial ruthenium ions (Ru^{3+}; Ru^{5+}) act as donors and acceptors leading to the fast transfer of photoinduced electrons from the conduction band of TiO_2 to dopant sites, which in turn reacts with adsorbed molecular oxygen producing superoxide anion radicals leading to more *OH radicals apart from the *OH radicals produced due to the trapping of holes generated in the valence band (h*). The generated *OH radicals react with the reactive dye (RR) solution resulting in the formation of non-polluted lower organic fragments.

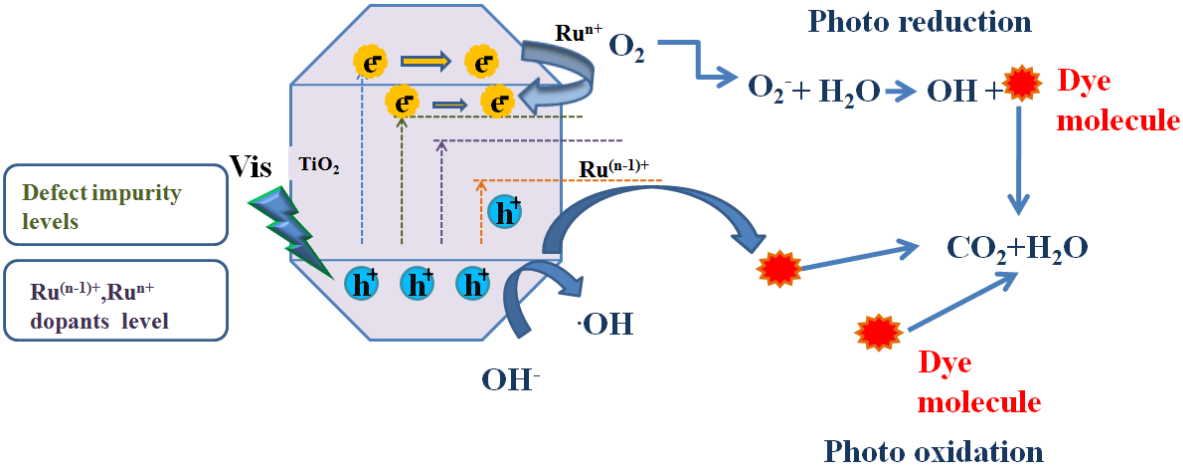

Fig.-8: These above graphics proposing the charge-transfer mechanism of TiO2 in the presence of Ru dopant to facilitate the visible-light-driven activity

Another possible mechanism of enhanced dye degradation in $Ru_XTi_{1-X}O_2$ samples could be attributed to the presence of Ru^{4+} ions in the TiO_2 crystal lattice that induces the strong acceptor ($Ru^{4+} \rightarrow Ru^{3+}+h^*$) transitions associated with a visible absorption band than the donor ($Ru^{4+} \rightarrow Ru^{5+}+e^-$) transitions [28]. Since the acceptor level of ruthenium ion (Ru^{4+}) is located slightly above the donor state and it is about ~1.9 eV above the valence band (VB) edge of TiO_2, the excitement of electron from the VB of TiO_2 takes place preferably to the acceptor level to the conduction band of TiO_2 on exposing the catalyst under the visible light. These light-induced electron transfer mechanism also generates significantly higher amount *OH radicals resulting in enhanced dye degradation rate by doping the ruthenium in titania ($Ru_XTi_{1-X}O_2$)

samples. The effect of catalyst concentration on the dye degradation performance was also investigated and the results are displayed in Fig.-9 (a, b). As expected, the dye degradation performance increases with the catalyst concentration for the ruthenium doped titania ($Ru_XTi_{1-X}O_2$) samples by exposing the mixture under UV and visible light. Though, no significant variation in dye degradation performance is noted at higher catalyst concentration (0.4~1.0 g/Lt) exposed under UV or visible light, relatively better dye degradation behavior is noted under UV exposure, when the catalyst concentration is maintained at 0.2 g/Lt.[31]

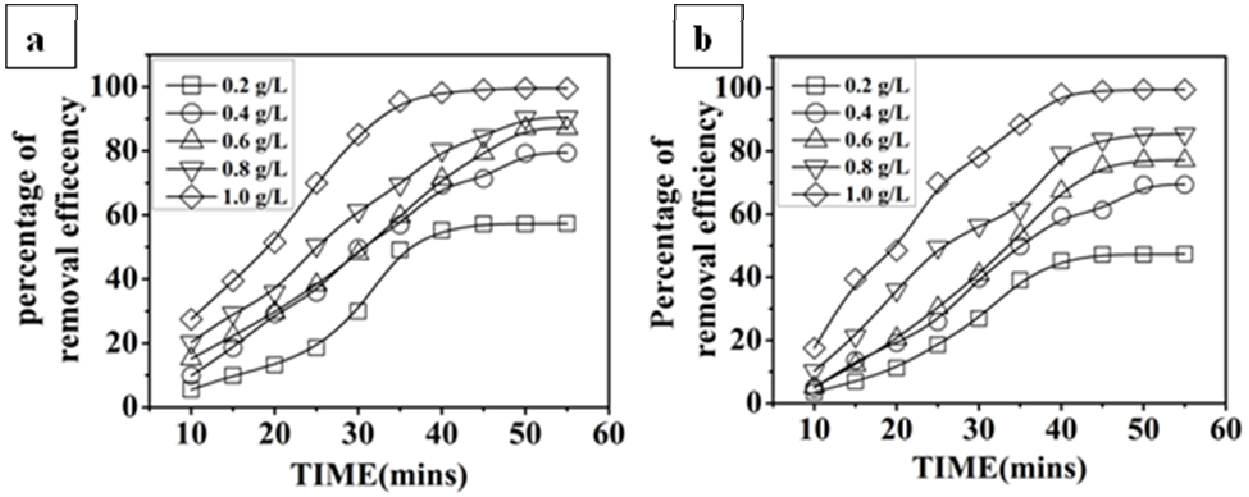

Fig.-9: The effect of catalyst concentration on the dye degradation under Visible/ Uv light

For instance, the dye degradation performance of $Ru_XTi_{1-X}O_2$ under UV light is about 50 %, whereas it is only 40 % under visible light radiation. Though the exact reason is unknown at this moment, one of the reasons could be the relatively lower content of interstitial ruthenium ions for visible light drove dye degradation performance.

CONCLUSION

In this work, successful one-pot hydrothermal synthesis of ruthenium doped titania nanosheets in the presence of a structure directing agents such as oleic acid and oleylamine have been presented. X-ray diffraction studies revealed the formation of both anatase and rutile type phases in the synthesized material. The presence of ruthenium ions both in the crystal lattice (Ru^{4+}) and in the interstitial positions (Ru^{3+}, Ru^{5+}) are corroborated using XRD, XPS and TEM. The influential role of the doped ruthenium on the visible light drove photocatalytic degradation has been unraveled. The variations in the band gap due to ruthenium doping as well as its role as donor/acceptors are responsible for the enhanced photocatalytic activity due to the facilitation of electron transfer mechanism under both UV and visible light.

ACKNOWLEDGEMENT

This experimental work has been carried out with support from the Department of Chemistry, School of Basic Sciences at Vels University, Chennai, Tamilnadu. The authors would like to thank Pandiyarasan Veluswamy for his contributions**.**

REFERENCES

1. Kudo and Y. Miseki, *Chem. Soc. Rev.*, **38**, 253(2009).
2. K. M. Agbekodo, B. Legube, S. Dard, *Water Res.*, **30**, 2535(1996).
3. S.D. Lambert, N. J. D. Graham, B.T.Croll, *Ozone Sci., Eng.***18**, 251–269 (1996).
4. A. Fujishima, T. N.Rao, D. A. Tryk, *Photocatalysis. J. Photochem. Photobiol. C: Photochem. Rev.*, **1**,1(2000).
5. Kubacka, M. Fernandez-Garcia, G. Colon, *Chem. Rev.*,**112**, 1555(2014).

6. X. Li, J. Yu, J. Low, Y. Fang, J. Xiao, and X. Chen, *J. Mater. Chem. A.*, **3**, 2485(2015).
7. R. Molinari, M. Borgese, E. Drioli, L. Palmisano, and M. Schiavello, *Catal. Today,* **75**, 77(2002).
8. G. Sagawe, R. J. Brandi, D. Bahnemann, and A.E. Cassano, *Chem. Eng. Sci.,* **58** (12), 2587(2003).
9. L. Korosi, I. Dekany, *Colloid Surf. A.*, **280**, 146(2006).
10. L. Korosi, S. Papp, J. Menesi, E. Illes, V. Zollmer, A. Richardt, and I. Dekany, *Colloid Surf. A.*, **319**, 136(2008)
11. M.K. Seery, R. George, P. Floris, and C. Pillai, *J. Photochem. Photobiol. A: Chem.*, **189** (2–3) ,258(2007).
12. H. E. Chao, Y. U. Yun, H.U. Xiangfang, and A. Larbot, *J. Eur. Ceram. Soc.*, **23**, 457(2003).
13. D. Bahnemann, *Sol. Energy.*, **77**, 445(2004).
14. S.G. Ullattil and P. Periyat, *Sol. Energy.*, **147**, 99(2017).
15. A. Bokare, M. Pai, A. Athawale*, Sol. Energy.*, **91**, 111(2013).
16. M. Sharma, T. Jain, S. Singh, O. P. Pandey, *Sol. Energy*,**86**, 626(2012).
17. V. Houskova, V. Štengl, S. Bakardjieva, N. Murafa, and V. Tyrpekl, *Appl. Catal. B: Environ.*, **89**, 613(2009).
18. M. Senthilnanthan, D. P. Ho, S. Vigneswaran, H. H . Ngo, and H.K. Shon, *Sep. Purif. Technol.*, **75**, 415(2010).
19. S. Nie, X.Zhao, and B. Liu, *RSC Adv.*, **5**,103386 (2015).
20. T. Nguyen-Phan, S. Luo, D. Vovchok, J. Llorca, S. Sallis, S. Kattel, W. Xu, L.F. J. Piper, D. E. Polyansky, S. D. Senanayake, D. Stacchiola, and J. Rodriguez, *Phys. Chem. Chem. Phys*.,**1**, 1(2016)
21. P. Roy, C. Das, K. Lee, R. Hahn, T. Ruff, M. Moll, and P. Schmuki, *J. Am. Chem. Soc.*,**133**, 5629(2011).
22. J.S. Chen, Y. L. Tan, C. M. Li, Y. L. Cheah, D. Luan, S. Madhavi, F. Y. C. Boey, L.A. Archer, and W. Lou, *J. Am, Chem. Soc.*, **132**, 6124(2010).
23. R. D. Shannon, *Acta Crystallogr., Sect. A.*, **32**, 751(1976).
24. C. D. Valentin, G. Pacchioni, and A. Selloni, *Phys. Rev. Lett.*, **97**, 166803 (2006).
25. Amrutashet and Vidyashetty, *Solar Energy*,**127**, 67(2016).
26. W. Q. Fang, X. L . Wang, H. Zhang, Y. Jia, Z. Huo, Z. Li, H. Zhao, H.G. Yang, and X. Yao, *J. Mater. Chem. A.*, **2**, 3513(2014).
27. G. Liu, H. G .Yang, X. Wang, L. Cheng, H. Lu, L. Wang, G. Q. Max Lu, and H. M . Cheng, *J. Phys. Chem. C.*, **113**, 21784(2009).
28. P. Triggs, and F. Levy, *Phys. Stat. Sol. B.*, **129**, 363(1985).
29. M.A. Fox, M.T. Dulay, *Heterogeneous Photocatalysis. Chem. Rev*., **93**(1), 341(1993).
30. K. Nagaveni, M.S. Hegde, N. Ravishankar, G.N. Subbanna, and Giridhar Madras, *Langmuir*, **20**, 2900(2004).
31. P. Salvador, C. Gutierrez, P. Triggs, and F. Levy, *Mater. Res. Bull.*, **19**, 634(1984).

[RJC-1969/2017]